JOURNAL OF APPLIED PHYSICS **112**, 123511 (2012)

High-pressure lattice dynamical study of bulk and nanocrystalline In_2O_3

B. Garcia-Domene,[1,2] H. M. Ortiz,[3,4,a)] O. Gomis,[1,5] J. A. Sans,[1,4] F. J. Manjón,[1,4,b)]
A. Muñoz,[1,6] P. Rodríguez-Hernández,[1,6] S. N. Achary,[7] D. Errandonea,[1,2]
D. Martínez-García,[1,2] A. H. Romero,[3,8] A. Singhal,[7] and A. K. Tyagi[7]
[1] *MALTA-Consolider Team*
[2] *ICMUV-Departamento de Física Aplicada, Universitat de València, 46100 Burjassot (València), Spain*
[3] *CINVESTAV-Departamento de Nanociencia y Nanotecnología, Unidad Querétaro, 76230 Querétaro, Mexico*
[4] *Instituto de Diseño para la Fabricación y Producción Automatizada, Universitat Politècnica de València, 46022 València, Spain*
[5] *Centro de Tecnologías Físicas, Universitat Politècnica de València, 46022 València, Spain*
[6] *Departamento de Física Fundamental II, Universidad de La Laguna, 38205 La Laguna, Tenerife, Spain*
[7] *Chemistry Division, Bhabha Atomic Research Centre, Mumbai-85, India*
[8] *Max-Planck-Institute für Mikrostrukturphysik, Weinberg 2, D-06120 Halle, Germany*

(Received 26 September 2012; accepted 13 November 2012; published online 19 December 2012)

The effect of pressure on the vibrational properties of bulk and nanocrystalline powders of cubic bixbyite-type In_2O_3 has been investigated at room temperature by means of Raman spectroscopy up to 31.6 and 30 GPa, respectively. We have been able to follow the pressure dependence of up to sixteen and seven Raman modes in bulk and nanocrystalline cubic In_2O_3, respectively. The experimental frequencies and pressure coefficients of the Raman-active modes of bulk cubic In_2O_3 at ambient pressure are in good agreement with those predicted by our theoretical *ab initio* calculations. Furthermore, a comparison of our experimental data with our calculations for the Raman modes in rhombohedral corundum and orthorhombic Rh_2O_3-II structures and with already reported Raman modes of rhombohedral corundum-type In_2O_3 at room pressure indicate that Raman scattering measurements provide no experimental evidence of the cubic to rhombohedral or cubic to orthorhombic phase transitions either in bulk material or in nanocrystals up to 30 GPa. © *2012 American Institute of Physics*. [http://dx.doi.org/10.1063/1.4769747]

I. INTRODUCTION

Indium oxide (In_2O_3) is an attractive semiconductor material that it is employed as a transparent conductive oxide in many industrial applications[1,2] because of its wide direct (3.75 eV) and indirect (3.10 eV) band-gaps[3–6] with additional high charge-carrier mobility. Due to these characteristics, In_2O_3 has been used in several applications like the production of solar cells,[7,8] light-emitting diodes,[9–11] liquid-crystal displays,[12,13] and gas sensors.[14–16] The improvement in performance of those applications and the development of new applications can also be envisaged in nanomaterials with controlled size and shape.[17–19] In this context, significant research efforts have been made for successful preparation of size-controlled In_2O_3 nanocrystals, hereafter named nano In_2O_3.[20–22]

At ambient conditions, In_2O_3 crystallizes in the cubic bixbyite-type structure (space group (SG) $Ia\bar{3}$, No. 206, $Z = 16$),[6,23] which is common to most rare-earth sesquioxides. However, several high-pressure phases are reported for this compound, like the rhombohedral corundum-type structure (SG $R\bar{3}c$, No. 167, $Z = 6$),[24] the orthorhombic Rh_2O_3-II structure (SG *Pbcn*, No. 60, $Z = 4$),[25] and the orthorhombic α-Gd_2S_3 structure (SG *Pnma*, No. 62, $Z = 4$).[26] In the cubic, rhombohedral, and Rh_2O_3-II structures, cations are sixfold-coordinated; however, cation coordination increases to seven and eight in the α-Gd_2S_3 structure. In recent years, the rhombohedral corundum-type structure of In_2O_3 has been synthesized at ambient conditions in a metastable way in different nanostructures and thin films.[27–40] In particular, the corundum phase is expected to show better properties than the bixbyite phase, like better stability and more conductivity;[6,41] therefore, it is of great interest to study the various pressure-induced phases of In_2O_3.

The properties of bulk bixbyite-type In_2O_3 have been thoroughly investigated at ambient conditions. In particular, its vibrational properties in bulk as well as in thin films have been studied since the 1970 s.[42–47] More recently, corundum-type In_2O_3 has been reported and characterized at ambient conditions by Raman spectroscopy, evidencing the differences between the Raman-active modes of the cubic and rhombohedral phases.[28,37,48] On the other hand, the properties of In_2O_3 nanocrystals are receiving increasing attention in the last years, and recently, the vibrational properties of In_2O_3 nanostructures have started to be also investigated.[49,50]

As regards the studies of bulk cubic In_2O_3 under pressure, it has been reported that cubic In_2O_3 retains its cubic structure till 6 GPa and 1450 °C;[51] on the other hand, it has been reported that In_2O_3 subjected to pressures of 6.5 GPa and temperatures between 880 and 1300 °C result in the growth of rhombohedral In_2O_3 when retrieved at ambient conditions.[24,52] The rhombohedral phase of In_2O_3 has also

---

[a] On leave from Departamento de Física, Universidad Distrital "Francisco José de Caldas," 110311 Bogotá, Colombia.

[b] Author to whom correspondence should be addressed. Electronic mail: fjmanjon@fis.upv.es.

TH-2012-64

been found by applying shock waves in the pressure range of 15–25 GPa to cubic In_2O_3.[53] More recently, Yusa *et al.* observed by x-ray diffraction (XRD) measurements the Rh_2O_3-II phase as post corundum phase in In_2O_3 at 7 GPa and 1900 K and the α-Gd_2S_3 phase as post-Rh_2O_3-II phase above 40 GPa and 2000 K.[25,26] Finally, Liu *et al.* carried out both powder XRD and Raman spectroscopy studies up to 27.8 and 26.2 GPa, respectively. They have shown that the compound remains stable up to 15.3 GPa, when it undergoes a phase transition to the corundum structure.[54] On the other hand, In_2O_3 nanocrystals have been less studied under pressure than bulk In_2O_3. In particular, Qi *et al.* performed powder XRD measurements up to 40 GPa at room temperature in In_2O_3 nanocrystals with average size of 6 nm. They showed that cubic In_2O_3 nanocrystals remain stable to 23.6 GPa, pressure at which they undergo a phase transition to the corundum structure.[22]

In this paper, we report Raman scattering measurements of bulk and nanocrystalline powders of cubic In_2O_3 at ambient temperature. Unlike previous works that report the existence of six Raman-active modes out of the twenty-two expected ones,[46,47,54] we show up sixteen (seven) Raman-active modes of the cubic phase in bulk (nano) In_2O_3. Additionally, we report the pressure dependence of the Raman-active mode frequencies of the cubic phase in bulk (nano) up to 31.6 (30.0) GPa. Both the frequencies at ambient pressure and the pressure coefficients measured for the Raman-active modes of the cubic phase are in good agreement with our lattice-dynamics *ab initio* calculations in the bulk material. We will show that our Raman scattering measurements do not provide clear evidence of the cubic to rhombohedral or cubic to orthorhombic phase transitions either in bulk material or in nanocrystals up to 30 GPa.

II. EXPERIMENTAL DETAILS

Commercial indium oxide powder (99.99% pure) from Sigma-Aldrich Inc. and as-grown nanocrystals of In_2O_3 were used in this work. The nanocrystals of In_2O_3 were prepared by nonhydrolytic alcoholysis ester elimination reaction of indium acetate in a procedure similar to that reported earlier.[21] Starting reagents for the preparation were indium acetate, oleyl alcohol, oleic acid, and methanol. About 0.5 mg of indium acetate along with 40 ml oleyl alcohol and 2.5 ml of oleic acid were taken in a 100 ml volume three-necked flask. The reaction flask was evacuated to a vacuum level of 2 mbar and heated slowly to 100 °C and held for 1 h. After the evacuation, the vacuum was cut off and slowly argon was introduced to the reaction flask. The reaction system was heated to 220 °C under flowing argon atmosphere and maintained at this temperature for 4 h. The reaction solution was then cooled to 60 °C, and excess of methanol (40 ml) was added to precipitate the nanocrystals. The precipitate was separated by centrifugation.

In_2O_3 nanocrystalline powder was characterized at ambient pressure by powder XRD collected on a Panalytical X-pert pro diffractometer using CuKα radiation (Figure 1). All the observed reflections can be attributed to cubic-In_2O_3 with a unit cell parameter $a = 10.1214(8)$ Å and volume $V = 1036.9(2)$ Å^3. The obtained unit cell parameter and volume are in agreement with those reported earlier in the literature.[21,55] The size of crystallites of nano In_2O_3 was obtained from the full width at half maximum (FWHM) of the (222) Bragg peak using the Scherrer relation with a shape factor of 0.9. The average crystallite size of the nanocrystals is about 9 ± 3 nm.

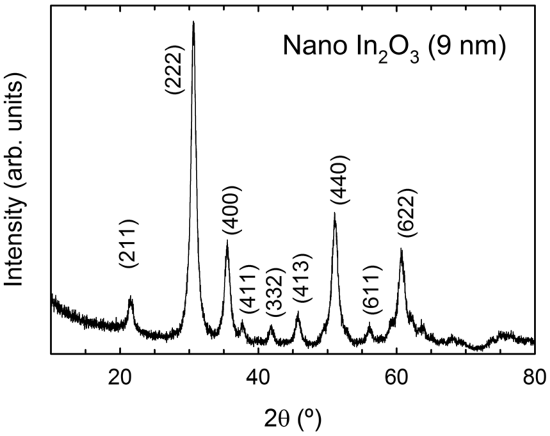

FIG. 1. X-ray diffraction data of nanocrystalline In_2O_3 obtained at 1 atm.

Raman scattering measurements were performed at room temperature in a backscattering geometry using the 632.8 nm laser line and a Horiba Jobin-Yvon LabRam HR UV spectrometer in combination with a thermoelectrically cooled multichannel CCD detector with a resolution below 2 cm^{-1}. High-pressure Raman measurements in bulk and nanocrystalline powders of In_2O_3 up to 31.6 and 30 GPa, respectively, were performed in a membrane-type DAC using a 50× large working distance objective and laser power below 10 mW. We used a mixture of methanol-ethanol-water in the proportion 16:3:1 as a quasihydrostatic pressure-transmitting medium and a few ruby balls of about 2 μm in diameter evenly distributed in the pressure chamber as a pressure sensor. The pressure was determined using the ruby fluorescence scale.[56] The experimental phonons have been analyzed by fitting, when possible, Raman peaks with a Voigt profile (Lorentzian convoluted with a Gaussian) where the Gaussian linewidth (1.5 cm^{-1}) has been fixed to the experimental setup resolution.

III. *AB INITIO* CALCULATIONS DETAILS

We have performed *ab initio* total-energy calculations within the density functional theory (DFT)[57] using the plane-wave method and the pseudopotential theory with the Vienna *ab initio* simulation package (VASP).[58–61] We have used the projector-augmented wave scheme (PAW)[62,63] implemented in this package to take into account the full nodal character of the all-electron charge density in the core region. Basis set including plane waves up to an energy cutoff of 520 eV were used in order to achieve highly converged results and accurate description of the electronic and dynamical properties. The description of the exchange-correlation energy was described with the generalized gradient approximation (GGA) with the PBEsol prescription.[64] A dense special k-points sampling for the Brillouin Zone (BZ) integration was performed in order to obtain very well converged energies and forces. At each selected volume, the structures were fully relaxed to their equilibrium configuration through the calculation of the forces and the stress tensor. It allows to obtain the relax structures at the theoretical pressures defined by the calculated stress. In the relaxed equilibrium configuration, the forces on the atoms are less than 0.006 eV/Å, and the deviation of the stress tensor from a diagonal hydrostatic form is less than 1 kbar (0.1 GPa). The application of DFT-based total-energy calculations to the study of semiconductors properties under high pressure has been reviewed in Ref. 65, showing that the phase stability, electronic, and dynamical properties of compounds under pressure are well described by DFT.

We have also performed lattice dynamics calculations of the phonons at the zone center (Γ point) of the BZ. Our theoretical results enable us to assign the Raman modes observed for the different phases. Furthermore, the calculations provide information about the symmetry of the modes and polarization vectors. Highly converged results on forces are required for the calculation of the dynamical matrix. We use the direct force constant approach.[66] The construction of the dynamical matrix at the Γ point of the BZ is particularly simple and involves separate calculations of the forces in which a fixed displacement from the equilibrium configuration of the atoms within the *primitive* unit cell is considered. Symmetry aids by reducing the number of such independent displacements, reducing the computational effort in the study of the analyzed structures considered in this work. Diagonalization of the dynamical matrix provides both the frequencies of the normal modes and their polarization vectors. This allows us to identify the irreducible representation and the character of the phonons modes at the Γ point.

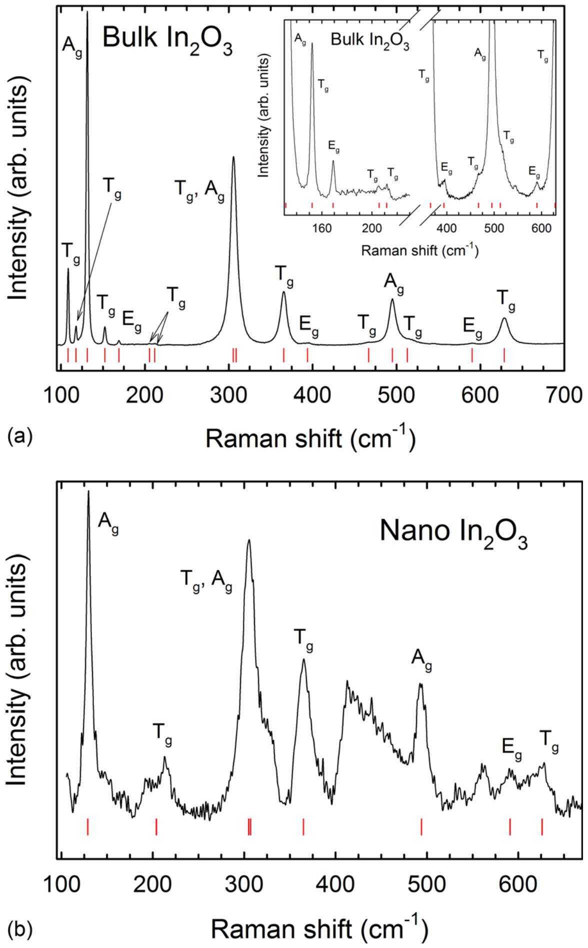

FIG. 2. (a) Unpolarized Raman scattering spectrum of bulk In_2O_3 at room conditions. Inset: Show the spectral regions with smaller intensity Raman modes. (b) Unpolarized Raman scattering spectrum of In_2O_3 nanocrystal. Vertical red lines show the theoretically predicted Raman-mode frequencies at room pressure for bulk In_2O_3 that have been observed experimentally.

IV. RESULTS AND DISCUSSION

Since the primitive cell of cubic In_2O_3 contains 8 formula units, group theory predicts that this structure should have 120 vibrational modes with the following representation:

$$\Gamma = 4A_g(R) + 4E_g(R) + 14T_g(R) + 5A_u + 5E_u + 17T_u(IR),$$

where *E* and *T* (also noted *F* in the literature) modes are double and triple degenerated, respectively. The 22 gerade (g) modes are Raman-active (R) modes, 16 T_u modes are infrared (IR)-active modes, the A_u and E_u are silent modes, and one T_u mode corresponds to acoustic vibrations.

Figures 2(a) and 2(b) show unpolarized Raman spectra at room temperature in bulk and nano In_2O_3, respectively. Unlike previous works where a maximum of seven Raman modes (109, 135, 305, 366, 495, 513, and 629 cm^{-1}) have been observed,[46,47,50,54] we have observed up to sixteen Raman-active modes of bulk cubic In_2O_3 powder at room conditions. The Raman spectrum is dominated by the stretching mode at 131 cm^{-1} and by the broad mode at 306 cm^{-1}. Table I summarizes the zero-pressure experimental frequencies and pressure coefficients of the Raman-active modes in bulk and nano In_2O_3. Our frequencies at ambient pressure are in good agreement with the theoretical frequencies of the Raman-active modes obtained from our *ab initio* calculations and with the Raman-active modes already reported in the literature.[42,46,47,50] Furthermore, thanks to our *ab initio* calculations we have assigned the symmetry of the different observed Raman modes [see Figs. 2(a) and 2(b)]. As regards nano In_2O_3, only seven modes have been clearly observed at ambient pressure. Their frequencies are rather close to those of bulk In_2O_3, as can be seen in Table I, since our nanoparticles have around 9 nm and phonon confinement effects are likely negligible for particles above 4 nm.[67]

Figures 3(a) and 3(b) show selected Raman spectra of bulk In_2O_3 at different pressures and the pressure dependence of the Raman mode frequencies up to 31.6 GPa, respectively. On the other hand, Figs. 4(a) and 4(b) show selected Raman spectra of nano In_2O_3 at different pressures and the pressure dependence of the Raman mode frequencies up to 30 GPa, respectively. When comparing Figs. 3(a) and 4(a), one can appreciate that the Raman spectra of bulk In_2O_3 have better quality than that of nano In_2O_3. In both bulk and nano In_2O_3, all Raman-active mode frequencies increase with pressure in a monotonous way till the maximum pressure attained in the experiment. Therefore, apparently, no

TABLE I. Experimental Raman-mode frequencies at room pressure and their pressure coefficients in bulk and nanocrystalline cubic In_2O_3. Experimental parameters have been obtained by fitting measured data to linear $\left(\omega = \omega_0 + \left(\frac{d\omega}{dP}\right)P\right)$or quadratic$\left(\omega = \omega_0 + \left(\frac{d\omega}{dP}\right)P + \left(\frac{d^2\omega}{dP^2}\right)P^2\right)$ expressions. Theoretical Raman-mode frequencies at room pressure and their pressure coefficients in bulk cubic In_2O_3 along with previously reported Raman-mode frequencies at room pressure are also shown for comparison.

	Raman modes of cubic In_2O_3									
	Ab initio calculations			In_2O_3 bulk powder			Nanocrystals of In_2O_3			Literature
Mode (Sym)	ω_0 (cm^{-1})	$\frac{\partial\omega}{\partial P}\left(\frac{cm^{-1}}{GPa}\right)$	$\frac{\partial^2\omega}{\partial P^2}\left(\frac{cm^{-1}}{GPa^2}\right)$	ω_0 (cm^{-1})	$\frac{\partial\omega}{\partial P}\left(\frac{cm^{-1}}{GPa}\right)$	$\frac{\partial^2\omega}{\partial P^2}\left(\frac{cm^{-1}}{GPa^2}\right)$	ω_0 (cm^{-1})	$\frac{\partial\omega}{\partial P}\left(\frac{cm^{-1}}{GPa}\right)$	$\frac{\partial^2\omega}{\partial P^2}\left(\frac{cm^{-1}}{GPa^2}\right)$	ω_0 (cm^{-1})
T_g	106 (1)	0.01 (1)	−0.008 (2)	108 (1)	0.07 (3)	−0.006 (2)				109[50]
T_g	114 (1)	0.3 (1)	−0.006 (2)	118 (1)	0.4 (1)	−0.009 (3)				
A_g	128 (1)	0.8 (1)	−0.009 (3)	131 (1)	1.0 (1)	−0.02 (1)	129 (2)	1.2 (1)	−0.03 (1)	131,[47] 135[47,50]
T_g	148 (1)	1.2 (1)	−0.01 (1)	152 (1)	1.4 (1)	−0.02 (1)				
E_g	165 (1)	1.1 (1)	−0.008 (2)	169 (1)	0.8 (1)					
T_g	199 (1)	1.8 (1)	−0.02 (1)	205 (3)	1.3 (1)					
T_g	204 (1)	1.5 (1)	−0.01 (1)	211 (3)	3.0 (2)					
T_g	302 (2)	2.2 (2)	−0.01 (1)	306 (2)	2.4 (2)	−0.03 (1)	306 (3)	2.5 (2)	−0.03 (1)	306,[46,47] 307,[47,50] 308[42]
A_g	302 (2)	3.1 (2)	−0.03 (1)	306 (2)	4.0 (3)	−0.06 (2)	307 (3)	3.3 (2)	−0.02 (1)	
E_g	308 (2)	3.1 (2)	−0.02 (1)							
T_g	312 (2)	2.6 (2)	−0.02 (1)							
T_g	356 (3)	3.9 (3)	−0.03 (1)	365 (2)	4.3 (3)	−0.06 (2)	365 (5)	4.9 (3)	−0.08 (3)	365,[42,47,49] 366[46,50]
T_g	379 (3)	3.9 (3)	−0.03 (1)							
E_g	385 (3)	3.6 (3)	−0.02 (1)	396 (4)	3.3 (2)					
T_g	438 (3)	3.0 (3)	−0.02 (1)							
T_g	447 (3)	4.3 (3)	−0.03 (1)	467 (4)						
A_g	476 (4)	3.4 (3)	−0.02 (1)	495 (2)	3.7 (3)	−0.04 (1)	494 (3)	3.8 (2)	−0.03 (1)	495,[46,47,50] 496,[47] 504[42]
T_g	499 (4)	5.0 (3)	−0.03 (1)	513 (4)						
T_g	520 (4)	4.7 (3)	−0.02 (1)							
E_g	565 (4)	5.2 (3)	−0.03 (1)	590 (4)	5.2 (4)		591 (6)	3.1 (4)		
A_g	576 (4)	5.4 (3)	−0.03 (1)							602[47]
T_g	600 (4)	5.4 (3)	−0.03 (1)	628 (2)	6.0 (2)	−0.09 (3)	626 (6)	5.4 (4)		627,[47] 628,[49] 630,[46] 631,[50] 637[42]

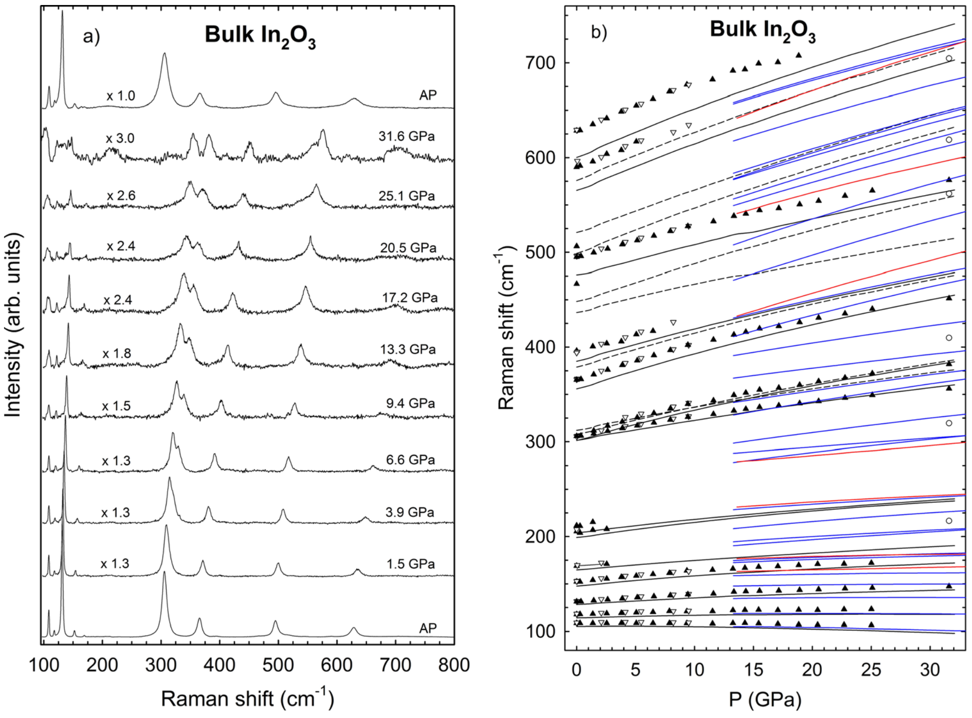

FIG. 3. (a) Selected Raman spectra of bulk In_2O_3 at different pressures up to 31.6 GPa. (b) Pressure dependence of the Raman-mode frequencies of bulk In_2O_3. Symbols correspond to experimental data. Filled (empty) black triangles up (down) correspond to upstroke (downstroke). Empty circles correspond with new peaks observed at 31.6 GPa, not related to the cubic phase. Black solid (dashed) lines represent theoretical data for observed (not observed) Raman-active modes in bulk In_2O_3. Red (blue) lines are theoretical data for Raman-active modes of the rhombohedral corundum (orthorhombic Rh_2O_3-II) phase in bulk In_2O_3.

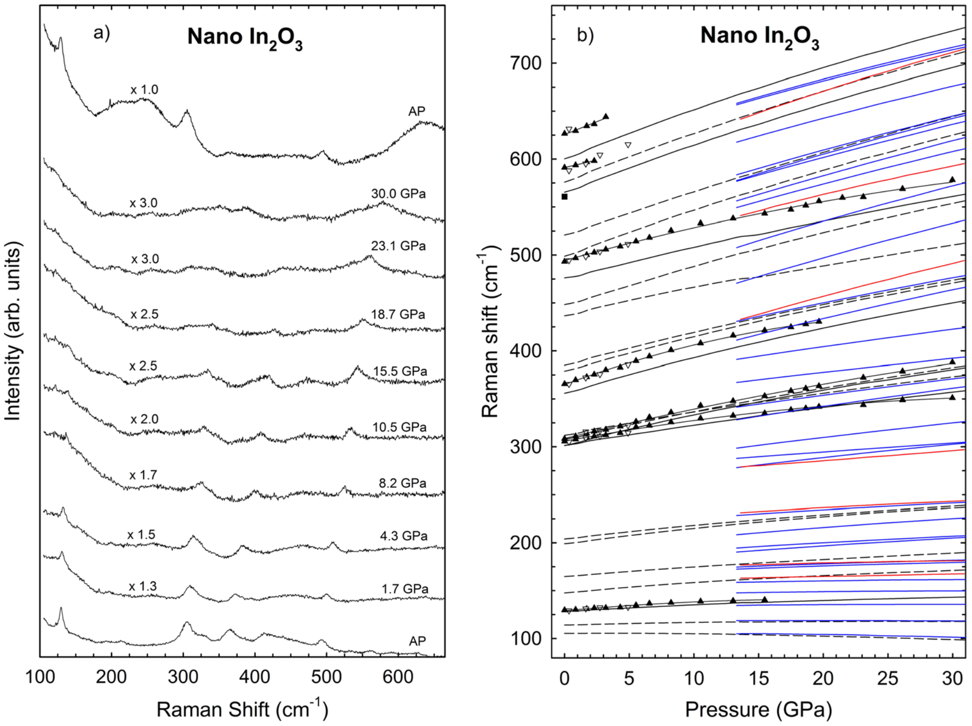

FIG. 4. (a) Selected Raman spectra of In_2O_3 nanocrystals at different pressures up to 30 GPa. (b) Pressure dependence of the Raman-mode frequencies of In_2O_3 nanocrystals. Symbols correspond to experimental data. Filled (empty) black triangles up (down) correspond to upstroke (downstroke). Filled black square (around 560 cm^{-1}) do not correspond to a first-order Raman mode. Black solid (dashed) lines represent theoretical data for observed (not observed) Raman-active modes in bulk In_2O_3. Red (blue) lines are theoretical data for Raman-active modes of the rhombohedral corundum (orthorhombic Rh_2O_3-II) phase in bulk In_2O_3.

phase transition seems to occur neither in bulk nor in nano In_2O_3 up to 30 GPa. Furthermore, on releasing pressure, the Raman spectrum of bulk In_2O_3 is similar to the initial one but with peaks slightly broadened. A similar Raman spectrum but with less defined features was obtained in the recovered sample of nano In_2O_3 at room pressure. It can be also observed that the peak widths of the Raman modes in the nanocrystalline sample are much larger than in the bulk leading to a possible overlapping of several Raman-active modes.

Figures 3(b) and 4(b) show the experimental pressure dependence of the first-order Raman-active mode frequencies for bulk and nano In_2O_3, respectively. These figures also include the theoretical pressure dependence of the Raman-active modes in the bulk bixbyite phase for comparison. As observed, most of the Raman modes exhibit a non-linear blue-shift with pressure, which is also in good agreement with our *ab initio* calculations up to the highest pressure attained in these experiments. Most of the Raman modes show a sublinear dependence of the frequency vs. pressure till 30 GPa, which is not observed when frequency is plotted vs. the relative volume variation, $\Delta V/V_0$, (not shown). This result suggests that the Gruneisen parameter of the Raman modes in cubic In_2O_3 is almost constant along the pressure range between ambient pressure and 30 GPa. Therefore, this means that there is no change in the force of the bondings what suggests that there is no charge redistribution between In and O atoms up to 30 GPa. Additionally, it can be appreciated that all the calculated frequencies are slightly underestimated due to the underestimation of the cohesion energy in the GGA approximation. The underestimation of experimental frequencies by GGA calculations is less than 5%; therefore, higher frequencies show larger experimental-theoretical differences than lower frequencies.[68] On the basis of the comparison of our experimental and theoretical frequencies, we propose that the peaks of the Raman-active modes centred at 395.8 and 589.7 cm^{-1} should have E_g symmetry [see Fig. 2(a)]. Similarly, the symmetry proposed for the Raman-active mode in In_2O_3 nanocrystals centred in 591.1 cm^{-1} is also E_g [see Fig. 2(b)].

An interesting feature of the Raman spectra of bulk In_2O_3 is the splitting of the broad peak near 306 cm^{-1} into two peaks, observed for pressures above 1.5 GPa. The broadening of this peak is evident in the Raman spectrum at 3.9 GPa [see Fig. 3(a)]. According to our calculations up to four Raman-active modes should appear in the region near 300 cm^{-1} for the cubic phase of In_2O_3. Note that out of the four predicted Raman modes in this region, three have similar pressure coefficients while the lowest in frequency has a smaller pressure coefficient (see Fig. 3(b) and Table I). Therefore, we ascribe the splitting observed above 1.5 GPa to two Raman-active modes of the cubic phase almost degenerate in frequency at room pressure that have very different pressure coefficients. In nano In_2O_3 [Fig. 4(b)], the splitting of the broad peak at 306 cm^{-1} was observed above 4 GPa; i.e., later than for bulk In_2O_3. A possible explanation for this behavior could be the larger overlapping of the two modes near 306 cm^{-1} in nanocrystals compared to the bulk, which prevents the observation of this splitting at smaller pressures.

In a previous work, Liu *et al.* observed the splitting of the modes near 306 cm^{-1} above 12.2 GPa and attributed it to the onset of a phase transition from the cubic bixbyite-type to the rhombohedral corundum-type structure.[54] With this interpretation, their high-pressure Raman scattering data matched with the observation of a new XRD peak above 15.3 GPa that they attributed to the rhombohedral phase. Furthermore, both experimental results seemed to agree with prior theoretical predictions that considered that a cubic-to-rhombohedral phase transition could be observed in In_2O_3 above 3.8 GPa.[6] Curiously, the observation of the cubic-to-rhombohedral phase transition was also claimed in a recent paper both on bulk and 6-nm-size nanocrystals.[22] However, our theoretical calculations do not predict the cubic-to-rhombohedral phase transition up to around 15 GPa in good agreement with previous calculations of Gurlo *et al*.[38] Furthermore, in agreement with Gurlo *et al.*, we have found that our calculations predict the cubic-to-orthorhombic Rh_2O_3-II phase transition to occur at pressures even lower than those for the cubic-to-rhombohedral transition; however, no report for the cubic-to-orthorhombic pressure-induced phase transition has been claimed at room temperature to our knowledge. Therefore, we consider that the splitting of the two Raman modes near 306 cm^{-1} as pressure increases does not constitute an evidence of the phase transition of In_2O_3 from the cubic-to-rhombohedral phase transition since this splitting is expected for two degenerate modes of the cubic phase at ambient pressure according to our *ab initio* calculations.

A curious feature of the Raman spectra of bulk In_2O_3 at different pressures is that, despite there is a general decrease of intensity of the Raman modes with increasing pressure, there is an increase of the relative peak intensity of the peak at 495 cm^{-1} with respect to the most intense A_g peak near 105 cm^{-1}. This behaviour contrast with that of other peaks that decrease in intensity or even disappear at low pressures. It can be noted that a broad band appears as a shoulder in the low-frequency side of the 495 cm^{-1} peak above 9.4 GPa. In fact, similar broad bands, but less clearly observed, are also developed above 9.4 GPa in the low-frequency side of the peaks at 306 and 365 cm^{-1}. Similar broad bands were already reported by Liu *et al.* above 12.8 GPa and were attributed to the onset of a phase transition to the rhombohedral phase with some disorder, as it was previously observed in corundum-type Ga_2O_3.[69] However, we must highlight that these bands do not correspond to Raman-active modes predicted by our theoretical calculations neither for the cubic phase nor for the rhombohedral or orthorhombic phases. Furthermore, we must note that neither our Raman spectra nor those obtained by Liu *et al.* above 15 GPa resemble to those measured for the rhombohedral phase of In_2O_3 at ambient pressure.[28,37] Therefore, on the basis of our Raman scattering measurements, our lattice dynamics calculations and the experimental evidence of Raman modes of the rhombohedral phase at ambient conditions, we cannot confirm either the cubic-to-rhombohedral or the cubic-to-orthorhombic phase transitions below 30 GPa but just the existence of some features that suggest the onset of a phase transition to an unknown structure.

Taking into account *ab initio* calculations, one could explain the observation of two XRD peaks near 6.4° and 9° above 15 GPa in both bulk and nanocrystals[22,54] and the absence of new Raman modes around that pressure by invoking that they are signs of the onset of a phase transition to the rhombohedral phase. However, a rather high kinetic barrier occurs for the cubic-to-rhombohedral or cubic-to-orthorhombic phase transitions.[70,71] In fact, data of previous authors show that the phase transition is far from complete even at 30 GPa.[22,54] In this sense, high kinetic barriers would allow the cubic phase being present at least till 30 GPa. Additionally, if the polarizability of the corundum phase is smaller than that of the cubic phase, the Raman scattering of the corundum phase could be of smaller intensity than that of the cubic phase and this would explain the absence of Raman-active modes of the corundum phase above 15 GPa while XRD peaks of the high-pressure phase are observed above that pressure.

Finally, we have to mention that several new Raman peaks are observed in the spectrum of bulk In_2O_3 at 31.6 GPa whose frequencies are plotted in Fig. 3(b) with open circles. These peaks are too weak to be clearly identified with any possible high-pressure phase; however, they indicate that, as far as Raman scattering concerns, the phase transition seems to take place above 30 GPa. We need to reach higher pressures to shed more light on the nature of the pressure-induced phase transitions in In_2O_3 at room temperature.

V. CONCLUSIONS

We report an accurate Raman spectrum at room conditions of bulk cubic In_2O_3, showing up to sixteen Raman-active modes. Thanks to *ab initio* calculations we have been able to assign the symmetry of most of the observed Raman-active modes in bulk and nanocrystalline cubic In_2O_3. We have also reported the pressure dependence of the Raman-active mode frequencies of the cubic phase in both bulk and nanocrystalline In_2O_3 up to 31.6 and 30 GPa, respectively. The pressure dependence of the experimental Raman modes shows a considerable non-linear pressure dependence that matches with the theoretical predictions. We have found no clear sign of a phase transition to the rhombohedral corundum-type structure neither in the bulk nor in the nanocrystals of cubic In_2O_3 till 30 GPa. Instead, we have found a considerable broadening of some Raman modes above 15 GPa that could be indicative of the onset of a phase transition. New modes appear in the Raman spectrum of bulk In_2O_3 above 30 GPa that seem to indicate that the phase transition occurs above this pressure in this compound at room temperature.

ACKNOWLEDGMENTS

Research financed by the Spanish MEC under Grant No. MAT2010-21270-C04-01/03/04 and from Vicerrectorado de Investigación de la Universitat Politècnica de València under Projects UPV2011-0914 PAID-05-11 and UPV2011-0966 PAID-06-11. CONACyT Mexico under the Project J-152153-F and the Marie-Curie Intra-European Fellowship have supported AHR. Supercomputer time has been provided by the Red Española de Supercomputación (RES) and the MALTA cluster. B.G.-D. acknowledges J. Ruiz-Fuertes for enlightening suggestions. We also acknowledge the financial support from the MEC through the FPI program and Juan de la Cierva fellowship.

[1] C. G. Granqvist, Appl. Phys. A **57**, 19 (1993).
[2] H. Mizoguchi and P. M. Woodward, Chem. Mater. **16**, 5233 (2004).
[3] P. D. C. King, T. D. Veal, F. Fuchs, Ch Y. Wang, D. J. Payne, A. Bourlange, H. Zhang, G. R. Bell, V. Cimalla, O. Ambacher, R. G. Egdell, F. Bechstedt, and C. F. McConville, Phys. Rev. B **79**, 205211 (2009).

[4] I. Hotovy, J. Pezoldt, M. Kadlecikova, T. Kups, L. Spiess, J. Breza, E. Sakalauskas, R. Goldhahn, and V. Rehacek, Thin Solid Films **518**, 4508 (2010).

[5] P. Erhart, A. Klein, R. G. Egdell, and K. Albe, Phys. Rev. B **75**, 153205 (2007).

[6] S. Zh Karazhanov, P. Ravindran, P. Vajeeston, A. Ulyashin, T. G. Finstad, and H. Fjellvag, Phys. Rev. B **76**, 075129 (2007).

[7] A. J. Breeze, Z. Schlesinger, S. A. Carter, and P. J. Brock, Phys. Rev. B **64**, 125205 (2001).

[8] R. B. H. Tahar, T. Ban, Y. Ohya, and Y. Takahashi, J. Appl. Phys. **83**, 2631 (1998).

[9] X. Xirouchaki, G. Kiriakidis, T. F. Pedersen, and H. Fritzsche, J. Appl. Phys. **79**, 9349 (1996).

[10] C. W. Tang and S. A. Vanslyke, Appl. Phys. Lett. **51**, 913 (1987).

[11] J. H. Burroughes, D. D. C. Bradley, A. R. Brown, R. N. Marks, K. Mackay, R. H. Friend, P. L. Burns, and A. B. Holmes, Nature **347**, 539 (1990).

[12] B. H. Lee, I. G. Kim, S. W. Cho, and S. H. Lee, Thin Solid Films **302**, 25 (1997).

[13] S. F. Hsu, C. C. Lee, S. W. Hwang, and C. H. Chen, Appl. Phys. Lett. **86**, 253508 (2005).

[14] F. Favier, E. C. Walter, M. P. Zach, T. Benter, and R. M. Penner, Science **293**, 2227 (2001).

[15] T. Takada, K. Suzuki, and M. Nakane, Sens. Actuators B **13**, 404 (1993).

[16] M. Z. Atashbar, B. Gong, H. T. Sun, W. Wlodarski, and R. Lamb, Thin Solid Films **354**, 222 (1999).

[17] Z. F. Pu, M. H. Cao, Y. Jing, K. L. Huang, and C. W. Hu, Nanotechnology **17**, 799 (2006).

[18] A. P. Alivisatos, Science **271**, 933 (1996).

[19] M. A. El-Sayed, Acc. Chem. Res. **34**, 257 (2001).

[20] S. G. Chen, Y. F. Huang, H. N. Xiao, H. W. Liao, C. G. Long, C. Ye and Q. Xia, Mater. Lett. **61**, 1937 (2007).

[21] A. Singhal, S. N. Achary, J. Manjanna, O. D. Jayakumar, R. M. Kadam, and A. K. Tyagi, J. Phys. Chem. C **113**, 3600 (2009).

[22] J. Qi, J. F. Liu, Y. He, W. Chen, and C. Wang, J. Appl. Phys. **109**, 063520 (2011).

[23] M. Marezio, Acta Crystallogr. **20**, 723 (1966).

[24] C. T. Prewitt, R. D. Shannon, D. B. Rogers, and A. W. Sleight, Inorg. Chem. **8**, 1985 (1969).

[25] H. Yusa, T. Tsuchiya, N. Sata, and Y. Ohishi, Phys. Rev. B **77**, 064107 (2008).

[26] H. Yusa, T. Tsuchiya, J. Tsuchiya, N. Sata, and Y. Ohishi, Phys. Rev. B **78**, 092107 (2008).

[27] A. Gurlo, N. Barsan, U. Weimar, M. Ivanovskaya, A. Taurino, and P. Siciliano, Chem. Mater. **15**, 4377 (2003).

[28] D. Yu, S.–H. Yu, S. Zhang, J. Zuo, D. Wang, and Y. T. Qian, Adv. Funct. Mater. **13**, 497 (2003).

[29] M. Epifani, P. Siciliano, A. Gurlo, N. Barsan, and U. Weimar, J. Am. Chem. Soc. **126**, 4078 (2004).

[30] D. B. Yu, D. B. Wang, and Y. T. Qian, J. Solid State Chem. **177**, 1230 (2004).

[31] M. Sorescu, L. Diamandescu, D. Tarabasanu-Mihaila, and V. S. Teodorescu, J. Mater. Sci. **39**, 675 (2004).

[32] Y. F. Hao, G. W. Meng, C. H. Ye, and L. D. Zhang, Cryst. Growth Des. **5**, 1617 (2005).

[33] C. Hoon Lee, M. Kim, T. Kim, A. Kim, J. Paek, J. Wook Lee, S.-Y. Choi, K. Kim, J.-B. Park, and K. Lee, J. Am. Chem. Soc. **128**, 9326 (2006).

[34] C. Chen, D. Chen, X. Jiao, and C. Wang, Chem. Commun. **2006**, 4632 (2006).

[35] J. Q. Xu, Y. P. Chen, Q. Y. Pan, Q. Xiang, Z. X. Cheng, and X. W. Dong, Nanotechnology **18**, 115615 (2007).

[36] Z. Zhuang, Q. Peng, J. Liu, X. Wang, and Y. Li, Inorg. Chem. **46**, 5179 (2007).

[37] Ch. Y. Wang, Y. Dai, J. Pezoldt, B. Lu, Th. Kups, V. Cimalla, and O. Ambacher, Cryst. Growth Des. **8**, 1257 (2008).

[38] A. Gurlo, P. Kroll, and R. Riedel, Chem.-Eur. J. **14**, 3306 (2008).

[39] Y. Fan, Z. Li, L. Wang, and J. Zhan, Nanotechnology **20**, 285501 (2009).

[40] L.-Y. Chen, Z.-X. Wang, and Z.-D. Zhang, New J. Chem. **33**, 1109 (2009).

[41] A. Gurlo, M. Ivanovskaya, N. Barsan, and U. Weimar, Inorg. Chem. Commun. **6**, 569 (2003).

[42] W. B. White and V. G. Keramidas, Spectrochim. Acta, Part A **28**, 501 (1972).

[43] H. Sobotta, H. Neumann, G. Kuhn, and V. Riede, Cryst. Res. Technol. **25**, 61 (1990).

[44] N. V. Porotnikov and O. I. Kondratov, Zh. Neorg. Khim. **38**, 653 (1993).

[45] C. Vigreux, L. Binet, D. Gourier, and B. Piriou, J. Solid State Chem. **157**, 94 (2001).

[46] G. Korotcenkov, V. Brinzari, M. Ivanov, A. Cerneavschi, J. Rodriguez, A. Cirera, A. Cornet, and J. Morante, Thin Solid Films **479**, 38 (2005).

[47] C. Matei Ghimbeu, J. Schoonman, and M. Lumbreras, Ceram. Int. **34**, 95 (2008).

[48] Ch. Y. Wang, V. Cimalla, H. Romanus, Th. Kups, G. Ecke, Th. Stauden, M. Ali, V. Lebedev, J. Pezoldt, and O. Ambacher, Appl. Phys. Lett. **89**, 011904 (2006).

[49] Y. Zhang, J. Li, Q. Li, L. Zhu, X. Liu, X. Zhong, J. Meng, and X. Cao, Scr. Mater. **56**, 409 (2007).

[50] O. M. Berengue, A. D. Rodrigues, C. J. Dalmaschio, A. J. C. Lanfredi, E. R. Leite, and A. J. Chiquito, J. Phys. D: Appl. Phys. **43**, 045401 (2010).

[51] H. R. Hoekstra, Inorg. Chem. **5**, 754 (1966).

[52] R. D. Shannon, Solid State Commun. **4**, 629 (1966).

[53] T. Atou, K. Kusaba, K. Fukuoka, M. Kikuchi, and Y. Syono, J. Solid State Chem. **89**, 378 (1990).

[54] D. Liu, W. W. Lei, B. Zou, S. D. Yu, J. Hao, K. Wang, B. B. Liu, Q. L. Cui, and G. T. Zou, J. Appl. Phys. **104**, 083506 (2008).

[55] X. Tao, L. Sun, Z. Li, and Y. Zhao, Nanoscale Res. Lett. **5**, 383 (2010).

[56] K. Syassen, High Pressure Res. **28**, 75 (2008).

[57] P. Hohenberg and W. Kohn, Phys. Rev. **136**, B864 (1964).

[58] G. Kresse and J. Furthmuller, Comput. Mater. Sci. **6**, 15 (1996).

[59] G. Kresse and J. Furthmuller, Phys. Rev. B **54**, 11169 (1996).

[60] G. Kresse and J. Hafner, Phys. Rev. B **47**, 558 (1993).

[61] G. Kresse and J. Hafner, Phys. Rev. B **49**, 14251 (1994).

[62] P. E. Blochl, Phys. Rev. B **50**, 17953 (1994).

[63] G. Kresse and D. Joubert, Phys. Rev. B **59**, 1758 (1999).

[64] J. P. Perdew, A. Ruzsinszky, G. I. Csonka, O. A. Vydrov, G. E. Scuseria, L. A. Constantin, X. L. Zhou, and K. Burke, Phys. Rev. Lett. **100**, 136406 (2008).

[65] A. Mujica, A. Rubio, A. Munoz, and R. J. Needs, Rev. Mod. Phys. **75**, 863 (2003).

[66] K. Parlinski, Z. Q. Li, and Y. Kawazoe, Phys. Rev. Lett. **78**, 4063 (1997).

[67] Akhilesh K. Arora, M. Rajalakshmi, T. R. Ravindran, and V. Sivasubramanian, J. Raman Spectrosc. **38**, 604 (2007).

[68] F. J. Manjon, J. Lopez-Solano, S. Ray, O. Gomis, D. Santamaria-Perez, M. Mollar, V. Panchal, D. Errandonea, P. Rodriguez-Hernandez, and A. Munoz, Phys. Rev. B **82**, 035212 (2010).

[69] D. Machon, P. F. McMillan, B. Xu, and J. Dong, Phys. Rev. B **73**, 094125 (2006).

[70] Q. Guo, Y. Zhao, C. Jiang, W. L. Mao, and Z. Wang, Solid State Commun. **145**, 250 (2008).

[71] C. Meyer, J. P. Sanchez, J. Thomasson, and J. P. Itie, Phys. Rev. B **51**, 12187 (1995).